

**Laboratory Week 1 – Module  $\alpha_1$**

***Polymer Structures***

**Instructor: Meri Treska**

**OBJECTIVES**

- Understand structure of amorphous materials
- Learn principles of x-ray scattering from amorphous materials
- Determine the glass transition temperature of various methacrylate polymers, using differential scanning calorimetry (DSC)

**SUMMARY OF TASKS**

- 1) Perform x-ray scattering measurements on a series of amorphous methacrylate polymers and semicrystalline polyethylene
- 2) Interpret observed peaks in the scattering patterns for methacrylate polymers
- 3) Determine the average interchain distances for polyethylene and methacrylate polymers from x-ray scattering patterns
- 4) Perform DSC measurements on methacrylate polymers, and determine T<sub>g</sub>
- 5) Correlate the structure data with the glass transition temperature of the methacrylate polymers

## BACKGROUND

### Diffraction from Crystalline Materials of Finite Crystal Dimension

For crystalline materials, we learned that the periodic arrangement of atoms gives rise to constructive interference of scattered radiation having a wavelength  $\lambda$  comparable to the periodicity  $d$  when Bragg's law is satisfied<sup>1</sup>:

$$n\lambda = 2d \sin \theta \quad [1]$$

where  $n$  is an integer and  $\theta$  is the angle of incidence. Bragg's law implies that constructive interference occurs only at the exact Bragg angle and the Intensity vs.  $2\theta$  curve exhibits sharp lines of intensity. In reality, diffraction peaks exhibit finite breadth, due both to instrumental and material effects. An important source of line broadening is finite crystal size. In crystals of finite dimensions, there is only partial destructive interference of waves scattered from angles slightly deviating from the Bragg angle.<sup>1</sup>

This is illustrated in Fig. 1 below, which shows XRD patterns for two polycrystalline  $V_2O_5$  films with different average crystal sizes.

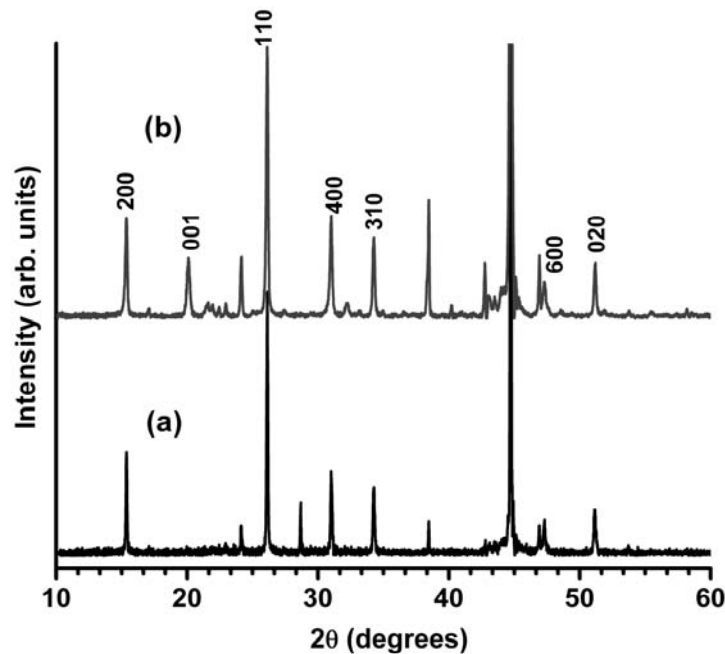


Figure 1. XRD patterns from  $V_2O_5$  thin films with average crystallite sizes of a) 250 nm and b) 80 nm. Peak broadening is observed with decreasing crystallite size. (data courtesy S. C. Mui)

If we define the angular width of a particular peak as:

$$B = \frac{1}{2}(2\theta_1 - 2\theta_2) \quad [2]$$

where  $\theta_1$  and  $\theta_2$  define the angular bounds of the peak in radians, then the average crystal size can be estimated from the Scherrer formula as<sup>1</sup>:

$$t = \frac{0.9\lambda}{B \cos \theta_B} \quad [3]$$

### **X-ray Scattering from Amorphous Materials**

Above it was established that as the crystal size gets smaller, diffraction peaks get broader. What happens in the extreme when there is no crystallinity? Whereas crystalline materials exhibit long range order, amorphous materials such as glassy polymers, metallic glasses and oxide glasses exhibit only *short range order*.<sup>2</sup> Their scattering pattern displays broad, low intensity peaks characteristic of the average local atomic environment, as shown in Fig. 2 for an amorphous zirconium phosphate<sup>3</sup>. *Applying the Scherrer formula to the peaks in this pattern, what is the calculated “crystal size” for this material? What do the peak positions represent?*

Figure removed due to copyright restrictions.

Figure 2. X-ray scattering pattern of amorphous zirconium phosphate synthesized using a non-ionic surfactant template.<sup>3</sup>

To better understand amorphous x-ray patterns, we can calculate the predicted intensity using the **structure factor** for amorphous materials. The structure factor is defined as<sup>2</sup>:

$$F(s) = \sum_{n=1}^M f_n \exp\left[2\pi i \vec{s} \cdot \vec{r}_n\right] \quad [4]$$

where  $\vec{s}$  is the scattering vector,  $f_n$  is the **atomic scattering factor** (proportional to atomic number), and  $\vec{r}_n$  is the atomic position vector for the  $n$ th atom. For a crystalline system, the summation in [4] is taken over the unit cell, and the total intensity is determined from the contribution of all unit cells.<sup>1</sup> For an amorphous material, there is no unit cell, since the atomic positions are not strictly periodic. Hence we take the summation in [4] over all atoms in the material.

Recalling the relationship between  $I_{coh}$  and  $F$ :

$$I_{coh} \propto F(s)F(s)^* = \sum_{m=1}^N \sum_{n=1}^N f_m f_n \exp\left[2\pi i \vec{s} \cdot \vec{r}_n\right] \exp\left[-2\pi i \vec{s} \cdot \vec{r}_m\right] \quad [5]$$

and letting  $\vec{r}_{nm} = \vec{r}_n - \vec{r}_m$ ,

$$I_{coh} = \sum_{m=1}^N \sum_{n=1}^N f_m f_n \exp\left[2\pi i \vec{s} \cdot \vec{r}_{nm}\right] \quad [6]$$

Using the assumption that the material is **isotropic**, i.e., that its structure has **radial symmetry**, the exponential can be replaced by its angular average<sup>2</sup>:

$$\int_0^\pi \int_0^{2\pi} \exp(2\pi i r_{nm} s \cos \alpha) \sin(\alpha) d\alpha d\phi = \frac{\sin(qr_{nm})}{qr_{nm}} \quad [7]$$

$$I_{coh} = \sum_{m=1}^N \sum_{n=1}^N f_m f_n \frac{\sin(qr_{nm})}{qr_{nm}} \quad [8]$$

where  $q = \frac{4\pi}{\lambda} \sin \theta = 2\pi s$  [9]

For simplicity, we consider the case where **all atoms** are of the **same type**:

$$I_{coh} = f^2 \sum_{m=1}^N \sum_{n=1}^N \frac{\sin(qr_{nm})}{qr_{nm}} \quad [10]$$

If we consider the interaction of each atom with itself,<sup>2</sup>

$$I_{coh} = f^2 N \left[ 1 + \sum_{n \neq m} \frac{\sin(qr_{nm})}{qr_{nm}} \right] \quad [11]$$

where the first term is individual atom scattering, obtained by letting  $r_{nm} \rightarrow 0$ .  $I_{coh}$  can be expressed in continuum form by substituting in the **radial distribution function**,

$4\pi r^2 \rho(r)$ :

$$I_{coh} = f^2 N \left[ 1 + \int_0^{\infty} 4\pi r^2 \rho(r) \frac{\sin(qr)}{qr} dr \right] \quad [12]$$

where  $\rho(r)$  is the *atomic pair density function*,<sup>3,6</sup> which gives the average density of atoms (number/volume) at a distance  $r$  from the center of a reference atom.<sup>2,4</sup> The quantity  $4\pi r^2 \rho(r) dr$  in eq. 12 gives the number of atoms within a shell of thickness  $dr$  around the reference atom, as shown in Fig. 3.

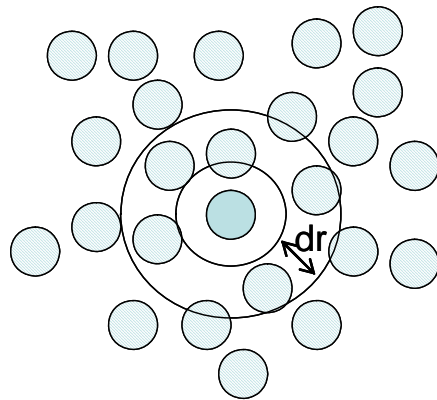


Figure 3. Schematic representation of atomic distribution within an amorphous material. The quantity  $4\pi r^2 \rho(r) dr$  is the number of atoms in a shell of thickness  $dr$  around a reference atom.

The atomic pair density function is related to the pair distribution function  $g(r)$ , by:<sup>2,4</sup>

$$g(r) = \frac{\rho(r)}{\rho_o} \quad [13]$$

where  $\rho_o$  is the bulk atomic density of the material (atoms/volume). For amorphous materials and liquids,  $g(r)$  has a form such as that shown in Fig. 4.<sup>5</sup> *How would this function look for a crystalline system?*

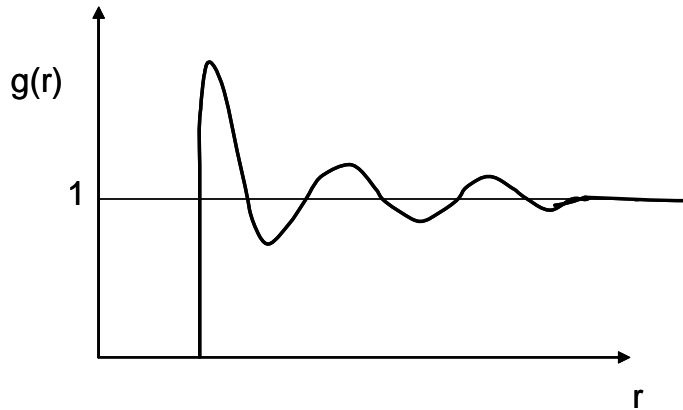


Figure 4. Schematic illustration of the pair distribution function for amorphous materials. The maxima correspond to distances where there is a higher probability of finding a neighboring atom.

The oscillatory behavior of  $g(r)$  gives rise similar oscillations in the scattering patterns from amorphous materials. From eq. [12] we can expect that the scattering intensity from an amorphous material will behave as a damped oscillatory function whose features depend on the average local spacing between atoms in the structure (Fig. 5).

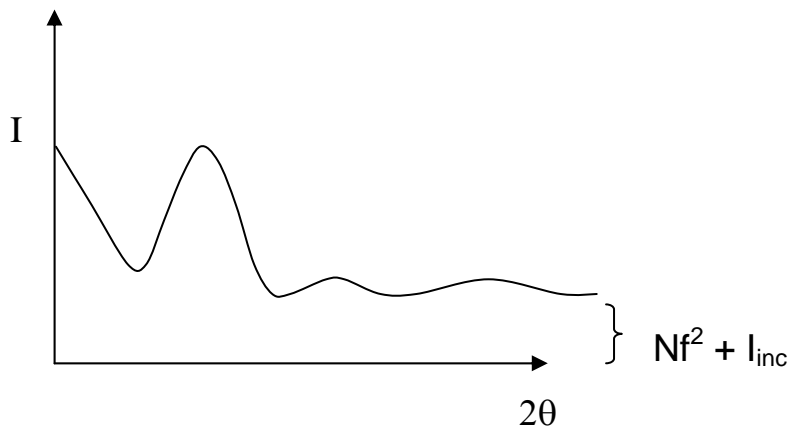


Figure 5. Schematic of X-ray scattering pattern for an amorphous material.

For systems that are partially crystalline, the amorphous and crystalline contributions to the scattering can be deconvoluted to determine the degree of crystallinity in the sample. The areas under the crystalline and amorphous peaks are proportional to their volume fraction in the sample,<sup>6</sup> as shown for the PP/P(E-co-VA) blend in Fig. 4.<sup>7</sup>

Figure removed due to copyright restrictions.

Figure 6. X-ray scattering pattern from blend of polypropylene and poly(ethylene-co-vinyl acetate). The total scattering pattern is deconvoluted into amorphous and crystalline contributions.<sup>7</sup>

### **Structure of polymers**

In this laboratory we will investigate the structure of polymers by X-ray scattering. Polymers are covalently bonded long chain molecules composed of repeating units made of carbon and hydrogen, and sometimes oxygen, nitrogen, sulfur, silicon and/or fluorine. The covalent bonding in polymers imposes directionality on their spatial arrangement into periodic structures. Polymer chains exhibit weak intermolecular forces due to van der Waals attractions. The ability of polymer chains to pack into an ordered array depends greatly on the stereoregularity of their pendant groups. For example, depending on the method of polymerization, polystyrene may exhibit isotactic, syndiotactic or atactic structure, as shown in Fig. 7. Atactic polystyrene is entirely

amorphous due to the random arrangement of the pendant phenyl groups, while syndiotactic and isotactic polystyrene, having more regular structures, exhibit crystallinity.

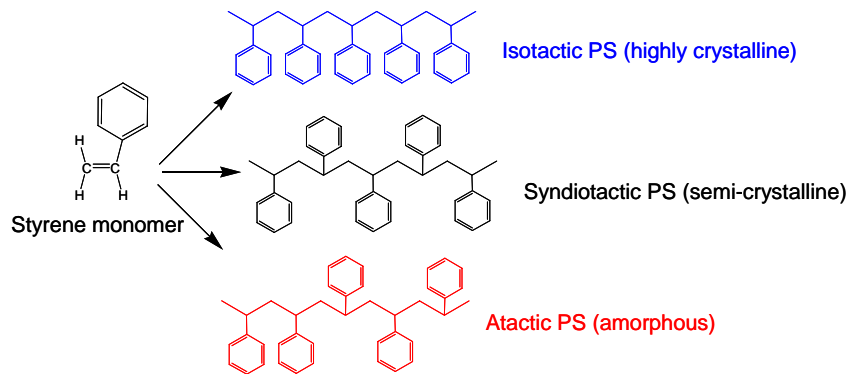


Figure 7. The three stereoisomers of PS: isotactic, syndiotactic, and atactic. Atactic polystyrene does not crystallize, due to the random placement of its side groups.

Polymers form into thin lamellar crystallites through a chain folding process, with their backbones oriented along one of the crystal axes, typically the c-axis. Chains may pack with zig-zag (all trans) or helical conformations of the backbone. Polyethylene, the largest volume commercial thermoplastic, arranges into an orthorhombic crystal with chains aligned along the c-axis in a zig-zag conformation (Fig. 8).<sup>6</sup>

Figures removed due to copyright restrictions.

Figure 8. Crystal structure of polyethylene.

For orthorhombic crystals, the d-spacing for a set of planes (hkl) is related to the lattice parameters through:<sup>1</sup>

$$d^{-2} = \frac{h^2}{a^2} + \frac{k^2}{b^2} + \frac{l^2}{c^2}$$

*Knowing the structure for PE, how can we determine the interchain distance from the x-ray diffraction data?*

For amorphous polymers, the scattering patterns show broad peaks representative of average characteristic distances between atoms in the structure. Most polymers exhibit a short range order maximum at a q value of  $1.4 \text{ \AA}^{-1}$ ,<sup>8,9</sup> as seen for several polymers in Fig. 9 below.

Figure removed due to copyright restrictions.

Figure 9. Normalized x-ray scattering intensity from 4 molten polymers. The peak at  $1.4 \text{ \AA}^{-1}$  is characteristic of the interchain van der Waals distance for C-C in amorphous hydrocarbon polymers. Oscillations at higher wavevectors are related to intrachain C-C distances.<sup>8</sup>

In this laboratory, we will compare the scattering patterns of a series of methacrylate polymers that have increasing side chain lengths. The general structure of these polymers is shown in Fig. 10. The length of the side chain influences the packing of these polymer chains in the melt or glassy state. As the side chain becomes longer, the average interchain distance increases.<sup>10</sup> This increased spacing between chain backbones results in a decrease in the glass transition temperature, the temperature at which chains begin to exhibit backbone mobility, transforming from the glassy to the rubbery state.

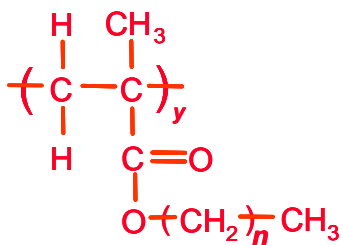


Figure 10. Monomer structure for methacrylate polymers.

Based on our X-ray scattering studies of various methacrylates, we will estimate the interchain spacing for the series of methacrylates, to correlate with glass transition values.

## WHAT IS GLASS TRANSITION? <sup>11,12,13,14</sup>

- A thermal property, characteristic of amorphous and semi-crystalline polymers.
- Identified by a characteristic temperature,  $T_g$  (the glass transition temperature), representing a transition of the polymer, from a “rubbery” or “leathery state” to a “glassy state”.
- Represents a change in the mechanical behavior of a polymer.

Below the  $T_g$ , a polymer is stiff, hard and brittle, and above the  $T_g$ , a polymer is pliable, soft, and tough.  
Changes in the elastic modulus.

- Manifestation of the changes in the mobility of the polymer chains.

- Above  $T_g$ , the long-range motion (i.e., the segmental motion) of the polymer chains is increased. e.g, chain bending, bond rotation about the segment ends. (Increase in the kinetic energy of the molecules).

- Below  $T_g$ , the chain mobility is suppressed.

Note: Polymer chains lack long-range translational motion.

- Represents changes in the thermodynamic properties of a polymer.

- Heat capacity changes
- Entropy changes
- A second order transition.

Involves a change in the heat capacity at  $T_g$ . No latent heat involved, as in the case of melting, which is a first order transition (discontinuous change in the heat capacity at the phase transition temperature).

- $T_g$  can vary over a wide range of temperatures (  $< - 100\text{ }^\circ\text{C}$  to  $> 100\text{ }^\circ\text{C}$  ) for various polymers.

### ***Some factors affecting $T_g$***

- Polymer structure (structural rigidity/ chain mobility)
  - Intermolecular forces (secondary forces of polymer chains)
  - Chemical composition
  - Molecular weight
- Experimental factors –
  - Processing
  - The rate of heating / cooling
  - Thermal history

## **EXPERIMENTAL TECHNIQUE:**

### **DIFFERENTIAL SCANNING CALORIMETRY [DSC] – TA INSTRUMENTS – MODEL Q100<sup>15</sup>**

DSC<sup>16</sup> is a thermal analysis technique useful for measuring thermal and thermodynamic properties of materials such as, the specific heat, melting and boiling points, glass transitions in amorphous/semi-crystalline materials, heats of fusion, reaction kinetics etc. The technique measures the temperature and the heat flow (in desired units, mW, W/g etc.) corresponding to the thermal performance of materials, both as a function of time, and temperature.

The TA Instruments DSC is a “HEAT FLUX” type system where the differential heat flux between a reference (e.g., sealed empty Aluminum pan) and a sample (encapsulated in a similar pan) is measured. The reference and the sample pans are placed on separate, but identical stages on a thermoelectric sensor platform

surrounded by a furnace. As the temperature of the furnace is changed (usually by heating at a linear rate), heat is transferred to the sample and reference through the thermoelectric platform. The heat flow difference between the sample and the reference is then measured by measuring the temperature difference between them using thermocouples attached to the respective stages.

The DSC provides qualitative and quantitative information on endothermic / heat absorption (e.g., melting), exothermic / heat releasing (e.g., solidification or fusion) processes of materials. These processes display sharp deviation from the steady state thermal profile, and exhibit peaks and valleys in a DSC thermogram (Heat flow vs. Temperature profile). The latent heat of melting or fusion can then be obtained from the area enclosed within the peak or valley. The glass transition is characterized by a steady change in the slope of the heat flow vs. temperature profile, with a corresponding change in the heat capacity of the material.

Some factors that may affect the DSC measurements are :

- Sample positioning on the DSC stage (variations in baseline)
- Structure and mass of the sample (proper thermal contact)
- Heating rate (Trade-off between sample attaining thermal equilibrium and data acquisition times. A fast heating rate may minimize the data acquisition time compromising salient features of the material property)

## **MATERIALS**

polymethyl methacrylate ( $T_g \sim 110^\circ\text{C}$ )

polyethyl methacrylate ( $T_g \sim 65^\circ\text{C}$ )

polypropyl methacrylate ( $T_g \sim 35^\circ\text{C}$ )

poly(n-butyl methacrylate) ( $T_g \sim 20^\circ\text{C}$ )

## **REFERENCES**

1. B.D. Cullity and S.R. Stock, *Elements of X-ray Diffraction*, 3<sup>th</sup> ed., Prentice Hall, NJ, 2001.
2. J. Zarzycki, *Glasses and the Vitreous State*, Cambridge University Press: Cambridge, UK, 1991, pp. 76-93.
3. G.L. Zhao, Z.Y. Yuan and T.H. Chen, Synthesis of amorphous supermicroporous zirconium phosphate materials by nonionic surfactant templating, *Mater. Res. Bull.* **40**, 1922 (2005).

4. S.J.L. Billenge and T. Egami, Short-range atomic structure of  $\text{Nd}_{2-x}\text{Ce}_x\text{CuO}_{4-y}$  determined by real-space confinement of neutron powder diffraction data. *Phys. Rev. B* **47**, 14386, (1993).
5. S.M. Allen and E.L. Thomas, *The Structure of Materials*, John Wiley & Sons, Inc: New York, 1999.
6. R.J. Young and P.A. Lovell, *Introduction to Polymers*, 2<sup>nd</sup> ed., Stanley Thornes Ltd: Cheltenham, UK, 1991.
7. M. Mihailova et al., X-ray investigation of polypropylene and poly(ethylene-co-vinyl acetate) blends irradiated with fast electrons. WAXS investigation of irradiated i-PP/EVA blends, *Radiation Phys. Chem.* **56**, 581 (1999).
8. M.-H. Kim, J.D. Londono and A. Habenschuss, Structure of molten stereoregular polyolefins with different side-chain sizes: linear polyethylene, polypropylene, poly(1-butene) and poly(4-methyl-1-pentene). *J. Poly. Sci. B: Poly. Phys.* **38**, 2480 (2000).
9. R.L. Miller and R.F. Boyer, Regularities in X-ray scattering patterns from amorphous polymers. *J. Poly. Sci. B: Poly. Phys.* **22**, 2043 (1984).
10. R.L. Miller and R.F. Boyer, X-ray scattering from amorphous acrylate and methacrylate polymers: evidence of local order. *J. Poly. Sci. B: Poly. Phys.* **22**, 2021 (1984).
11. P. Meares, *Polymers, Structure and Bulk Properties*, D. Van Nostrand Company, London, 1965.
12. G. Odin, *Principles of polymerization*, John Wiley and Sons, New York, 3<sup>rd</sup> edition, 1991
13. *Thermal Characterization of Polymeric Materials*, ed. E. A. Turi, Press, 1981
14. *Guidelines for Quantitative Studies – Heat Capacity Experiments*, TA Instruments Manual DSC 2920, 4-15.
15. K.L.RamKumar, M.K.Saxena, and S. B. Deb, Experimental Evaluation Of Procedures For Heat Capacity Measurements By Differential Scanning Calorimetry, *Journal of Thermal Analysis and Calorimetry*, **66**, 387, (2001)